Performance Evaluation of a Curved Type Vane Separator at Different Plate Spacings in the Range of 25 to 35mm Using Numerical Simulation

Rafee, Roohollah; Rahimzadeh, Hassan*[+]

Faculty of Mechanical Engineering, Amirkabir University of Technology,
P.O. Box 15875-4413 Tehran, I.R. IRAN

ABSTRACT: *In this paper, the turbulent air droplet flow inside a single passage of a curved type vane separator has been studied numerically. The simulation is based on the Eulerian - Lagrangian method. For turbulent air flow calculations, a computer code was developed to solve the Reynolds Averaged Navier Stokes (RANS) equations together with the equations of Reynolds Stress Transport Model (RSTM) on collocated unstructured meshes. Finite volume method was applied for discretization of the gas flow equations. Also, the low Reynolds modification has been applied for RSTM and the results have been compared with those obtained by Standard RSTM. For droplet trajectory calculation, the Eddy Interaction Model (EIM) was applied to take the turbulent dispersion of droplets into account. The performance of the code has been evaluated by comparing the simulations results with experimental data. The results show that by including the wall reflection terms in transport equations of the Reynolds stresses, better predictions can be achieved than those obtained by RSTM without wall reflection terms. The enhanced wall treatments can further improve the results. Finally, the pressure loss and droplet removal efficiency for different plate spacings have been calculated using the developed codes. The numerical results show that for plate spacings in the range of 25 mm to 35 mm, the pressure loss is approximately constant. On the other hand, the increment in plate spacing reduces the droplet removal efficiency. Therefore, in the mentioned range, 25mm spacing gives the best performance for this type of the vane separator.*

KEY WORDS: *Droplet dispersion, Eddy Interaction Model (EIM), Reynolds Stress Transport Model (RSTM), Enhanced wall treatment, Curved type vane separator.*

INTRODUCTION

Vane separators have a wide range of applications in industries. For example, they are used in scrubbers to capture the small droplets from natural gas streams. Numerical simulation of air droplet flow in such a device can help the designers to make the separators with the maximum removal efficiency and minimum pressure loss. The removal efficiency is defined by:

$$\eta = \frac{\text{Mass rate of the removed droplets}}{\text{Mass rate of the entering droplets}} \qquad (1)$$

The mass flow rate of droplets in vane separators is usually assumed to be less than 10% of air flow rate; therefore, the Eulerian-Lagrangian model can be used in numerical simulation. The main assumption is that droplets cannot affect the air flow. The inertia of the droplets makes them unable to change their direction at the bends of the vane separator, so they will be removed from the gas stream.

Three general approaches for simulating turbulent fluid flows are: Reynolds-averaged Navier–Stokes (RANS) equations method, Direct Numerical simulation (DNS) and Large Eddy Simulation (LES). The limitations of DNS and LES make them impractical for being applied to the large Reynolds numbers or in complex passages. For industrial applications of the flows with large Reynolds numbers in complex passages, RANS remains as the most commonly used approach. In this study, the air flow field is obtained by solving the RANS equations.

Some numerical works on mist eliminators have been carried out by *Verlaan* [1] and *Wang & Davies* [2]. *Galletti et al.* [3] made a numerical simulation using Shear Stress Transport (SST) model and compared the results with *Ghetti*'s work [4]. They also showed that SST turbulence model gives better results than standard k-ε model.

Jøsang & Melaaen [5] made an experimental investigation on a special curved type vane separator using the LDA technique.

For droplets size in the range of 1 to 50 μm, turbulent dispersion is very important. The Eddy Interaction Model (EIM) is extensively used to model the droplet dispersion and deposition in turbulent flows. In EIM, the influence of turbulence on droplets dispersion is taken into account by assuming that droplets are interacting with eddies which are characterized by their velocity, size and lifetime. The basic EIM assumes isotropic turbulence in order to calculate the instantaneous air velocities from mean flow quantities.

Because of isotropic turbulence assumption, the basic EIM cannot accurately describe the droplet dispersion and deposition in some regions in which the flow is strongly anisotropic. Some modifications based on k-ε turbulence model are proposed by *Kallio & Reeks* [6] and *Sommerfeld et al.* [7]. *Wang & James* [8] showed that the calculations based on these modifications are in good agreement with the experimental measurement, except for very small droplets. *James et al.* [9] used

the same modifications (called Varied EIM) to obtain the removal efficiency of wave plate mist eliminators with drainage channels. Without drainage channels, the deposited liquid can be gathered at the bend corners and may be re-entrained into the air stream, leading to a reduction in the droplet collection efficiency. *James et al.* [10] proposed a model for the generation and flow of liquid film that is formed in mist eliminators without drainage channels. They pointed out that the Reynolds number for the air flow in their case is approximately in the range of 4000 and 6000. *Launder & Spalding* [11] pointed that the turbulent flows with Reynolds numbers less than 20000 should be considered as low-Reynolds-number turbulent flows.

Recently, *Rafee et al.* [12] made a numerical simulation of airflow and droplet transport in a wave-plate (zigzag) mist eliminator. They concluded that the RSTM with enhanced wall treatment gives the better predictions of droplet removal efficiency than other turbulence models for that type of mist eliminator.

In the following sections, the governing equations for air flow and droplet motion and the relevant numerical schemes have been discussed in details. Then performance of the developed in-house code was investigated by comparing its results with the experimental and numerical data from *Jøsang & Melaaen*'s [13] work. They made a numerical simulation of air field using the Reynolds stress model with standard wall function. They did not include the wall reflection effects in pressure strain terms calculation in RSTM transport equations. They pointed out that in their simulation, the combination of the RSTM and highest order scheme (QUICK) for discretizatiom of the air flow equations on the unstructured grid gave the worst result. Their work showed that by using the mentioned combination, the pressure drop was over predicted by 50%. Then the calculated pressure loss will be compared for different plate spacings. Finally, the droplet removal efficiency of the separator is calculated and compared for different plate spacings.

GOVERNING EQUATIONS
Turbulent Air Flow

Jøsang & Melaaen [5] made an experimental setup to study the fluid flow inside a curved type vane separator by using Laser Doppler Anemometry (LDA). In their study the plate spacing was 25 mm. Their measurements
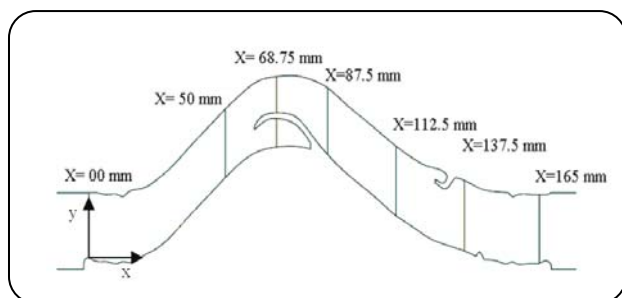
Fig. 1: Different positions of the measured profiles by Jøsang & Melaaen [5] in the vane separator.

positions are shown in Fig. 1. They also measured the pressure at 50 mm upstream of the inlet and 50 mm downstream of the outlet of the separator.

The air flow inside the mist eliminator is turbulent. The equations of turbulent air flow inside an eliminator (RANS and RSTM equations) can be expressed in the following generalized form:

$$\frac{\partial}{\partial t}(\rho\varphi) + \frac{\partial}{\partial x_k}(\rho U_k \varphi) = \frac{\partial}{\partial x_k}\left(\Gamma_\varphi \frac{\partial\varphi}{\partial x_k}\right) + S_\varphi \tag{2}$$

where φ is the general dependent variable, Γ_φ, is the diffusion coefficient and S_φ is the source term. The contents of φ, Γ_φ and S_φ are given in Table 1. *Jøsang & Melaaen* [13] described all of the terms for equations given in Table 1. In the present work the pressure strain terms, in Reynolds stresses transport equations are also modeled using the following decomposition (See *Launder & Shima* [14]):

$$\varphi_{ij} = \varphi_{ij,1} + \varphi_{ij,2} + \varphi_{ij,w} \tag{3}$$

where, $\varphi_{ij,1}$ is the slow pressure strain term, $\varphi_{ij,2}$ is the rapid pressure strain term and $\varphi_{ij,w}$ is the wall reflection term. The slow pressure strain term is modeled by:

$$\varphi_{ij,1} = C_1 \rho \frac{\varepsilon}{k}\left[R_{ij} - \frac{2}{3}\delta_{ij}k\right] \tag{4}$$

The rapid pressure strain term, $\varphi_{ij,2}$ is written as follows:

$$\varphi_{ij,2} = -C_2\left[P_{ij} - \frac{2}{3}\delta_{ij}G_k\right] \tag{5}$$

where $G_k = \frac{1}{2}P_{kk}$.

The wall reflection term damps the normal stress perpendicular to the wall and enhances the stresses parallel to the wall. *Launder & Shima* [14] proposed the following formula for wall reflection term:

$$\varphi_{ij,w} = \tag{6}$$

$$C_1'\frac{\varepsilon}{k}\left(R_{km}n_k n_m \delta_{ij} - \frac{3}{2}R_{ik}n_j n_k - \frac{3}{2}R_{jk}n_i n_k\right)\frac{C_l k^{3/2}}{\varepsilon y}$$

$$+C_2'\left(\varphi_{km2}n_k n_m \delta_{ij} - \frac{3}{2}\varphi_{ik,2}n_j n_k - \frac{3}{2}\varphi_{jk,2}n_i n_k\right)\frac{C_l k^{3/2}}{\varepsilon y}$$

where n_k is the x_k component of the unit normal vector to the wall and y is the normal distance to the wall and $C_1 = C_\mu^{3/4}/\kappa$ (where $C_\mu = 0.09$ and $\kappa = 0.4187$).

The transport equations and coefficients of the standard version of the RSTM are given by *Launder* [15] and *Lien & Leschziner* [16] and extensively used in the literature. For standard Reynolds stress without enhanced wall treatment, the constants of the above equations are given in Table 2.

When enhanced wall treatment for low Reynolds flow is applied, the pressure strain term must be modified. In this situation, the coefficients of C_1, C_2, C_1' and C_2' are computed by the following formulas proposed by *Launder and Shima* [14]:

$$C_1 = 1 + 2.58A_1\sqrt{A_2}(1 - e^{-(0.0067Re_t)^2}) \tag{7}$$

and:

$$C_2 = 0.75\sqrt{A_1} \tag{8}$$

and:

$$C_1' = -\frac{2}{3}C_1 + 1.67 \tag{9}$$

$$C_2' = \max\left[\frac{\frac{2}{3}C_2 - \frac{1}{6}}{C_2}, 0\right] \tag{10}$$

where:

$$Re_t = \frac{\rho k^2}{\mu\varepsilon} \tag{11}$$

$$A_1 = [1 - \frac{9}{8}(A_2 - A_3)] \tag{12}$$

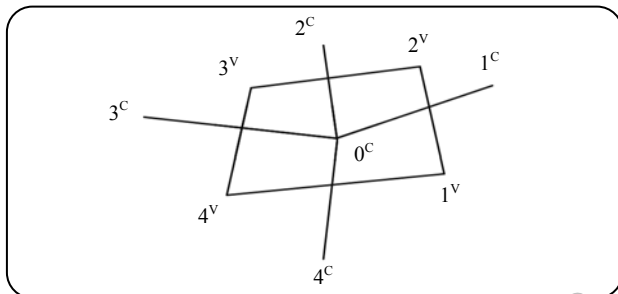$$A_2 = a_{ik}a_{ki} \tag{13}$$

97

Table 1: Contents of φ, Γ_φ and S_φ in general transport equation.

equation	φ	Γ_φ	S_φ
Continuity	1	0	0
momentum	U_i	μ	$-\dfrac{\partial p}{\partial x_i} + \dfrac{\partial}{\partial x_j}(-\rho R_{ij})$
Reynolds stress	R_{ij}	$\mu + \dfrac{\mu_t}{\sigma_k}$	$P_{ij} + \varphi_{ij} - \varepsilon_{ij}$
TKE Dissipation Rate	ε	$\mu + \dfrac{\mu_t}{\sigma_\varepsilon}$	$\dfrac{\varepsilon}{k}(C_{1\varepsilon}G_k - C_{2\varepsilon}\rho\varepsilon)$

Table 2: Constants for standard Reynolds stress model.

σ_k	σ_ε	$C_{1\varepsilon}$	$C_{2\varepsilon}$	C_μ	C_1	C_2	C'_1	C'_2
0.8	1.0	1.44	1.92	0.09	1.8	0.6	0.5	0.3

Fig. 2: Control volume and data structure used for discretization of the transport equation.

and:

$$A_3 = a_{ik}a_{kj}a_{ji} \tag{14}$$

And the Reynolds stress anisotropy tensor (a_{ij}) is defined by:

$$a_{ij} = -\left(\frac{-\rho R_{ij} + \frac{2}{3}\rho k\delta_{ij}}{\rho k}\right) \tag{15}$$

Finite Volume Discretization of the Air Flow Equations

By integrating Eq. (2) over a control volume (See Fig. 2) and using the divergence theorem, the general transport equation in integral form is obtained:

Details of discretization for convection and diffusion terms of Eq. (16) over the unstructured meshes are given by *Lien* [17] and *Rafee & Rahimzadeh* [18]. The same method was used here. For convection terms the second order upwind method has been used to increase the precision of the results.

In the steady problems, the discretized transport equation can be expressed as:

$$A_0\varphi_0 = \sum_{i=1}^{4} A_i\varphi_i - S_{p\varphi} + S_{d\varphi} - S_{c\varphi} + S_\varphi\Omega_0 \tag{17}$$

The pressure correction equation is derived from the integral form of the continuity equation and can be written as (See *Lien* [17], for example):

$$A_{0p}p'_0 = \sum_{i=1}^{4} A_{ip}p'_i - \sum_{i=1}^{4} C^*_{si} \tag{18}$$

where C^*_{si} is the mass flux over the ith surface of the cell before the pressure correction. The corrected pressure and velocity field can be calculated from

$$p = p^* + \alpha p' \tag{19}$$

$$u_0 = u_0^* - \frac{\Omega_0}{(A_0)_0}\left(\frac{\partial p'}{\partial x}\right)_0 \quad \text{and} \tag{20}$$

$$v_0 = v_0^* - \frac{\Omega_0}{(A_0)_0}\left(\frac{\partial p'}{\partial y}\right)_0$$

where, α is under the relaxation factor for p'. In this paper, the value of 0.1 is used as the relaxation factor for p'. The algorithm of solution is:

(1) Guessing the pressure field p

(2) Calculation of mass fluxes, coefficients and source terms.

(3) Calculation of velocities and other variables (Eq. (17)).

(4) Calculation of pressure correction (Eq. 18)

(5) Calculation of *p*, *u* and *v* from their starred values using the velocity correction formulas (Eqs. 19, 20)

(6) Returning to step (2), then repeating the whole procedure until a converged solution is obtained.

This is quite similar to SIMPLE method used by *Patankar* [19] for staggered grids.

Wall Boundary Condition

As Described before, two types of near wall treatment for RSTM are used in this study. The Standard wall functions can be implemented in the same manner described by *Jøsang & Melaaen* [13]. On the other hand, a combination of two-layer model with enhanced wall function is made as the enhanced wall treatment. For enhanced wall treatment, the definition of near wall region starts with the following equation:

$$\text{Re}_y = \frac{\rho y\sqrt{k}}{\mu} \tag{21}$$

98

where y is the distance from wall.

The turbulent kinetic energy (k) is computed using the equations of fully turbulent flow, but turbulent viscosity is computed from (*Jongen* [20]):

$$\mu_{t,enh} = \lambda_\varepsilon \rho C_\mu \frac{k^2}{\varepsilon} + (1 - \lambda_\varepsilon)\mu_{t,2layer} \tag{22}$$

where $\mu_{t,2layer}$ can be calculated using the *Wolfstein* [21] method:

$$\mu_{t,2layer} = \rho c_\mu L_\mu \sqrt{k} \tag{23}$$

The blending function (λ_ε) prevents the numerical solution from unwanted oscillation when fully turbulent Reynolds stress model does not match the two-layer model.

The length scale in the above equation is computed from:

$$L_\mu = y C_1^*(1 - e^{\frac{-Re_y}{A_\mu}}) \tag{24}$$

where $C_1^* = \kappa c_\mu^{3/4}$ and $A_\mu = 70$ and blending function (λ_ε) is obtained from:

$$\lambda_\varepsilon = \frac{1}{2}[1 + \tanh(\frac{Re_y - 200}{A_b})] \tag{25}$$

For $Re_y < 200$, the ε field is computed from

$$\varepsilon = \frac{k^{3/2}}{yC_1^*(1 - e^{\frac{-Re_y}{2C_1^*}})} \tag{26}$$

For wall adjacent cells the value of dimensionless velocity is given by following formula of *Kader* [22]:

$$u^* = e^{\Gamma_2} u_{laminar}^* + e^{\frac{1}{\Gamma_2}} u_{turbulent}^* \tag{27}$$

where the blending function is given by:

$$\Gamma_2 = \frac{-0.01y^{*4}}{1 + 5y^*} \tag{28}$$

$u_{laminar}^*$ is defined by:

$$u_{laminar}^* = y^* \tag{29}$$

And $u_{turbulent}^*$ is defined by:

$$u_{turbulent}^* = \frac{1}{k}\ln(Ey^*) \tag{30}$$

At the wall adjacent cell center, the equation of the standard wall function is used for computation of turbulent kinetic energy.

Droplet Motion Equations

Droplet motion in the wave plate mist eliminator has been studied by several authors. For example *Wang & James* [8]; *Galletti et al.* [3] and *Jøsang* [23] studied the droplet motion using the following assumptions:

I: the droplet concentration is low enough that the effects of droplets on the primary air flow and the droplet - droplet interaction can be ignored.

II: there is no turbulence modulation due to the presence of droplets.

III: density of air is much smaller than droplets, so the effects of virtual mass force, pressure gradient and basset history is negligible.

IV: *Galletti et al.* [3]; *Wang & James* [8]; *James et al.*, [9,10], *Chan and Golay* [24] and *Zhao et al.* [25] assumed the droplets can be treated as hard sphere particles. In this study, the effects of droplet distortion will be considered. By assuming the dilute flow of small droplets in the gas stream, if the effects of Saffman lift force, Brawnian force and the gravity force on droplets are taken into account, the equation of the motion is given by:

$$\frac{d\vec{u}_d}{dt} = \frac{\vec{u}_g - \vec{u}_d}{\tau_d} + \vec{F}_L + \vec{n}(t) + \vec{g} \tag{31}$$

Here, $\vec{u}_g$ and $\vec{u}_d$ are the velocities of the air flow and droplet, respectively, $\vec{F}_L$ is the lift force, $\vec{n}(t)$ is the Brawnian force and $\vec{g}$ is gravity acceleration vector. In this study the gravity acceleration has been taken into account. The method of time integration for above equation was described by *Wang & James* [8] the same method is adopted here. Also, $\vec{x}_d$ is the droplet position vector. The relaxation time of the droplet, τ_d, is defined by:

$$\tau_d = \frac{4d\rho_d C_c}{3\rho_g C_D |\vec{u}_g - \vec{u}_d|} \tag{32}$$

In the above equation, d is droplet diameter; ρ_d and ρ_g are the density of the droplet and the air, respectively. C_c is the Stokes-Cunningham slip correction (*He & Ahmadi*, [26]).

The drag coefficient (C_D) is determined by *Liu et al.* [27]:

$$C_D = C_{D_{sphere}}(1 + 2.632y_{CD}) \tag{33}$$

$C_{Dsphere}$ is calculated using the following formula (*Hinds* [28]):

$$C_{Dsphere} = \begin{cases} \dfrac{24}{Re_d} & Re_d \leq 1.0 \\ \dfrac{24}{Re_d}(1 + 0.15 Re_d^{0.687}) & Re_d > 1.0 \end{cases} \tag{34}$$

The droplet Reynolds number is defined by:

$$Re_d = \frac{\rho_g |\vec{u}_g - \vec{u}_d| d}{\mu_g} \tag{35}$$

In Eq. (33), y_{CD} is the droplet distortion which is determined by the solution of the following differential equation:

$$\frac{d^2 y_{CD}}{dt^2} = \frac{C_F}{C_b}\frac{\rho_g}{\rho_d}\frac{u^2}{r^2} - \frac{C_k \sigma}{\rho_d r^3}y_{CD} - \frac{C_{dy}}{\rho_d}\frac{\mu_d}{r^2}\frac{dy_{CD}}{dt} \tag{36}$$

where μ_d and σ_d are the droplet viscosity and surface tension respectively and C_F, C_b, C_d and C_k are the model constants given in Table 3 (See *Lamb*, [29]). In the above equation, *u* is the relative velocity between air and droplet and r is the droplet radius. The initial conditions of $y_{CD}(0)=0$ and $(dy_{CD}/dt = 0)$ are selected for solution.

The details for evaluation of the Saffman lift force and Brownian force were given by *He & Ahmadi* [26].

The instantaneous air velocity $\vec{u}_g$ in the above equations is defined by:

$$\vec{u}_g = \vec{U}_g + \vec{u}'_g \tag{37}$$

The fluctuating part of the air velocity ($\vec{u}'_g$) allows for the influence of turbulence on the motion of the droplets. Air flow field computations can provide mean velocities and Reynolds stresses, then Eddy Interaction Model (EIM) is used to construct the fluctuating components.

Varied eddy interaction model based on two equation turbulence models is popular (see *James et al.*, [9,10] and *Galletti et al.* [3]). Here, a version of varied EIM, using Reynolds stress model, is presented. By considering an air computational cell (Fig. 3), it is assumed that velocity fluctuation in each vertex can be obtained from:

Table 3: Model constants for calculation of droplet distortion (Lamb [29]).

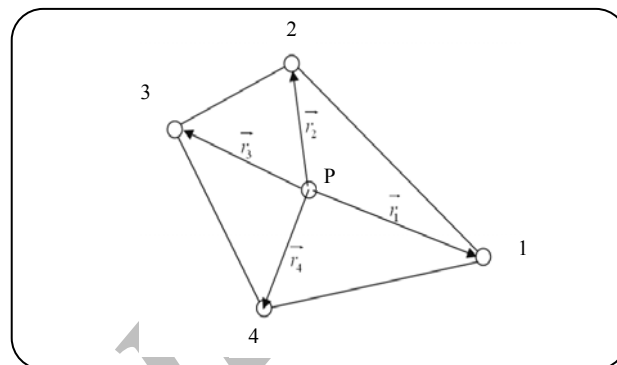| C_F	C_b	C_k	C_{dy}
0.333	0.5	8.0	5.0

Fig. 3: Droplet location at a computational air field cell (point P).

$$(u'_1, v'_1, w'_1) = \left(N_r \sqrt{R_{11}}, N_r \sqrt{R_{22}}, N_r \sqrt{R_{33}}\right) \tag{38}$$

Here, N_r is the random number. N_r is assumed constant during the droplet eddy interaction. This random number must be drawn from a normal distribution with zero mean and unity standard deviation.

The characteristic lifetime of Eddy is calculated by:

$$T_e = 0.201\frac{k_g}{\varepsilon_g} \tag{39}$$

At droplet position, the air field parameters such as k_g, ε_g and R_{11} must be calculated. For example, k_g at droplet location can be determined from :(see Fig. 3).

$$k_g = \alpha_1 k_1 + \alpha_2 k_2 + \alpha_3 k_3 + \alpha_4 k_4 \tag{40}$$

where

$$\alpha_i = \frac{|\vec{r}_i|}{|\vec{r}_1| + |\vec{r}_2| + |\vec{r}_3| + |\vec{r}_4|} \tag{41}$$

The Eddy length scale at droplet position is given by:

$$L_e = 0.164\frac{k_g^{3/2}}{\varepsilon_g} \tag{42}$$

where k_g and ε_g are turbulent kinetic energy and dissipation rate at droplet location.

If $L_e < \tau_d \left| \overrightarrow{u_g} - \overrightarrow{u_d} \right|$ then the droplet eddy interaction time is calculated from

$$T_i = -\tau_d \log\left[1 - \frac{L_e}{\tau_d \left| \overrightarrow{u_g} - \overrightarrow{u_d} \right|} \right] \qquad (43)$$

But, if $L_e \geq \tau_d \left| \overrightarrow{u_g} - \overrightarrow{u_d} \right|$, then the droplet becomes trapped in the eddy and

$$T_i = T_e \qquad (44)$$

During the droplet–eddy interaction U_g, u'_g , eddy life time and length scale is usually updated whenever the droplet crosses a cell boundary, but keeping N_r constant until the end of the interaction.

Time step size is calculated from:

$$\Delta t = \max(\frac{\tau_d}{5}, 10^{-6}) \qquad (45)$$

Grid Generation

Depth of Industrial vane separator is much larger than the other two dimensions, so the flow is assumed to be two-dimensional. The collection efficiency of the separator at each droplet size was determined from the ratio of total mass of removed droplets and injected droplets.

Grid dependency of the solution was tested by using different mesh sizes. For example, for the plate spacing of 25 mm, three meshes with total number of 20312 (mesh No.1), 39154 (mesh No.2) and 45468 (mesh No.3) quadrilateral cells were generated and used for simulations. The predicted profiles of u component of the mean velocity by using different meshes have been shown in Fig. 4. The results have been presented for the air bulk velocity of 3.54 m/s at x=112.5 mm. Since the results of mesh No.2 and mesh No.3 are almost equal, it can be concluded that the grid independent solution is obtained by using a mesh with 39154 quadrilateral cells and 40325 nodes. The mesh was generated with interval size of 0.0005 mm. Details of generated mesh have been shown in Fig. 5.

This mesh was used for both RSTM with standard wall function (hereinafter for convenience referred to as "Standard RSTM") and RSTM with enhanced wall treatment (hereinafter for convenience referred to as "Enhanced RSTM"). Details of the vane geometry are
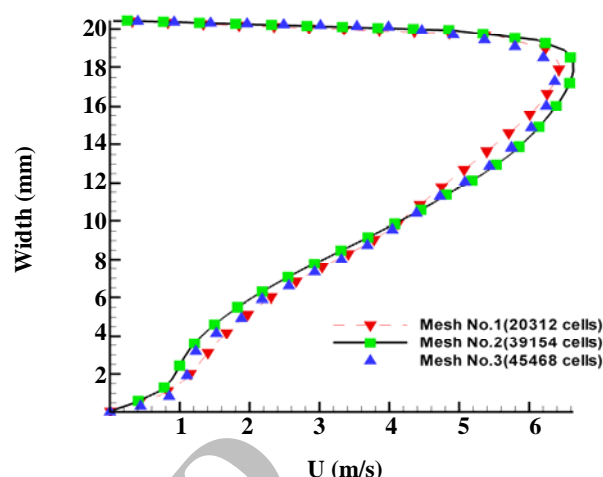

Fig. 4: The predicted profiles of u component of the mean velocity by using different meshes at x=112.5 mm for the air bulk velocity of 3.54 m/s.
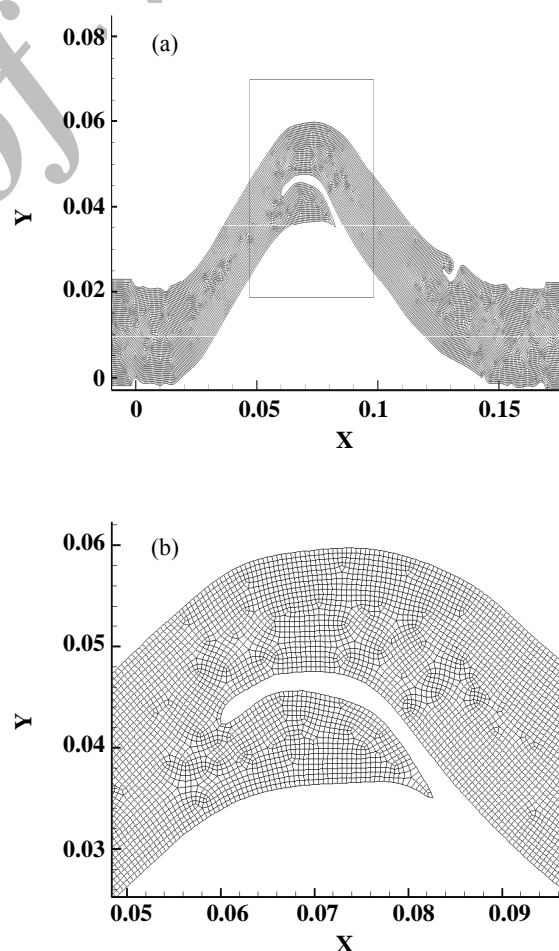

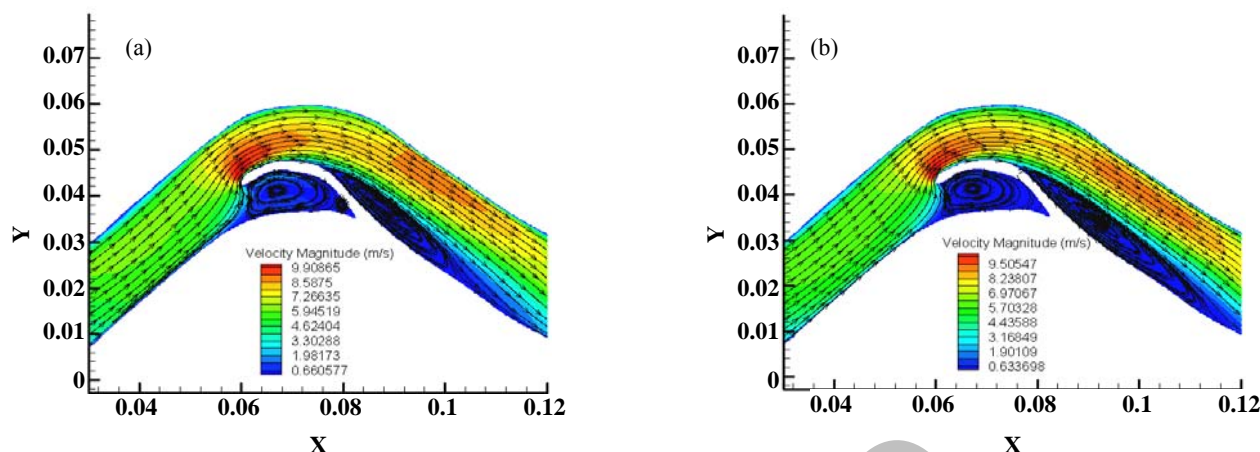*Fig. 5: Unstructured mesh generated for gas flow computation a) whole mesh b) details of mesh at bend.*

101

Fig. 6: The stream traces and velocity magnitude contours at the bulk air velocity of 3.54 m/s obtained by:
a) The Enhanced RSTM   b) The Standard RSTM

given in *Jøsang* PhD thesis [23]. The generated unstructured mesh for gas field computation is shown in Fig. 5-a and details of mesh at bend is shown in Fig. 5-b.

At the inlet, the uniform velocity of 2.46, 3.54 and 4.54 m/s, and the turbulence intensity of 5% are considered for simulation. For S=25 mm, the air flow Reynolds number will be 4094, 5892 and 7556, respectively. The gas flow Reynolds number is defined by:

$$Re = \frac{\rho VS}{\mu} \tag{46}$$

Where V is the mean velocity of the gas flow and S is the plate spacing.

Two straight ducts with the length of 1.0 and 0.5 m are considered as inlet and outlet piece.

In the following sections, first the results of the simulations are compared with the experimental and numerical data of *Jøsang & Melaaen's* [13] study to select an appropriate turbulence model. Then the results of numerical simulations for different plate spacings are presented. Finally, this model is used for droplets trajectory calculation and predicted droplet removal efficiency curves are compared for different plate spacings.

RESULTS AND DISCUSSION
Gas Flow Simulation

In Fig. 6-a and Fig. 6-b, the stream traces and velocity magnitude contours obtained by the Enhanced RSTM have been compared with the results of the Standard RSTM for 25 mm plate spacing. The Standard RSTM

predicts a larger dead zone after the drainage channel. These results are obtained at the air bulk velocity of 3.54 m/s.

For more discussion and to select the proper turbulence model, profiles of u-component of the mean velocity at different sections of the separator have been compared with experimental data in Figs. 7a, 7b, 7c and 7d. By applying the wall reflection term in the RSTM model, the better predictions for mean velocity profile can be achieved. Also it is evident that RSTM with enhanced wall treatment gives better results than the other models.

In Fig.s 8a, 8b, 8c and 8d, the attained profiles of the x-rms velocity at different sections have been shown.

The Enhanced RSTM results are in better agreement with the results of the experimental data. Here, the results of the Standard RSTM (with or without wall reflection terms) have more deviation from the measured profiles. As described before, in EIM the rms velocities play an important role in small droplet tracking because the fluctuating velocities are obtained by using the rms velocities (see Eq. 45). Therefore the selected turbulence model must predict correct rms velocities.

Jøsang & Melaaen [5] also measured the pressure 50 mm upstream of the inlet and 50 mm downstream of the vane inlet. In table 4, the calculated pressures drop obtained from different turbulence models are compared with their measurements. The results of *Jøsang & Melaaen's* [13] simulations are also presented in this table. Here, the Enhanced RSTM prediction is the closest value to the experiments.
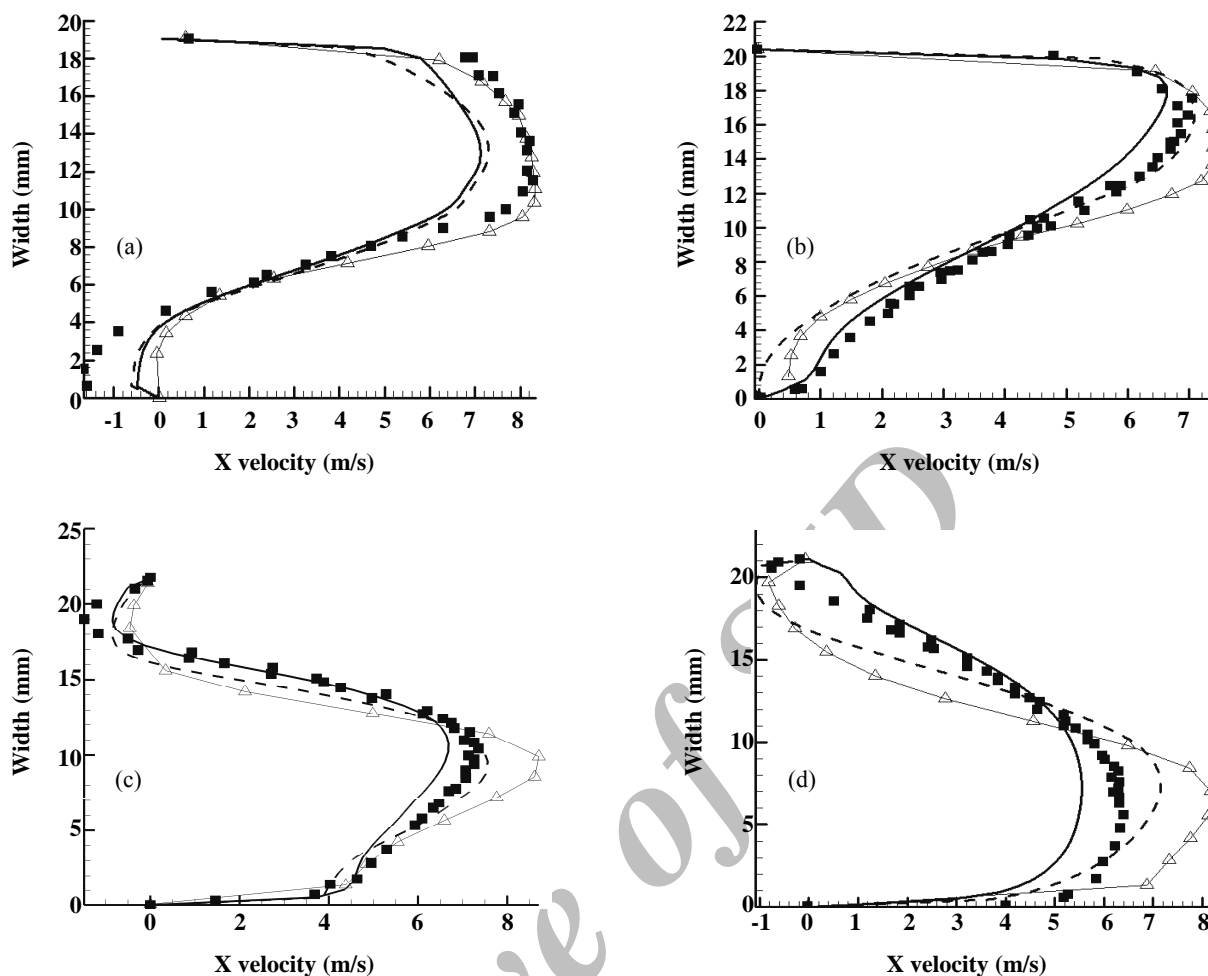
102

Fig. 7: Profile of u component of mean velocity at the bulk air velocity of 3.54 m/s:
a) at x=87.5 mm   ,   b) at x= 112.5 mm   ,   c) at x=137.5 mm   ,   d) at x=165 mm.

The pressure loss has been calculated by using the following formula:

$$\Delta P = \frac{\int\limits_{at\ inlet} P dy}{\int\limits_{at\ inlet} dy} - \frac{\int\limits_{at\ outlet} P dy}{\int\limits_{at\ outlet} dy} \tag{47}$$

Among the models, the RSTM with enhanced wall treatment gives the best prediction for the pressure loss. Therefore the RSTM with enhanced wall treatment has been selected to study the effects of changing the plate spacing on the performance of the vane separator.

In Fig. 9, the predicted pressure loss for three different bulk gas velocities have been compared with the measurements of *Jøsang* [23]. This figure shows the ability of the Enhanced RSTM in prediction of the air flow quantities inside the separator.

To study the effects of plate spacings on the performance of the separator, seven different models with the spacings of 17, 20, 23, 26, 30, 35 and 40 mm were provided. In Fig. 10, the calculated pressure loss versus plate spacing for three different air bulk velocities has been demonstrated. Each curve appertains to a constant air bulk velocity. As can be seen, by increasing the plate spacing from 17 mm to 25 mm, first the pressure loss will decrease with a large slope. However, it remains approximately constant over the range of the 25 mm to 35 mm for plate spacing. Further raise in plate spacing will decrease the pressure loss. However, there is an upper limit for plate spacing because for spacings greater than 48 mm,
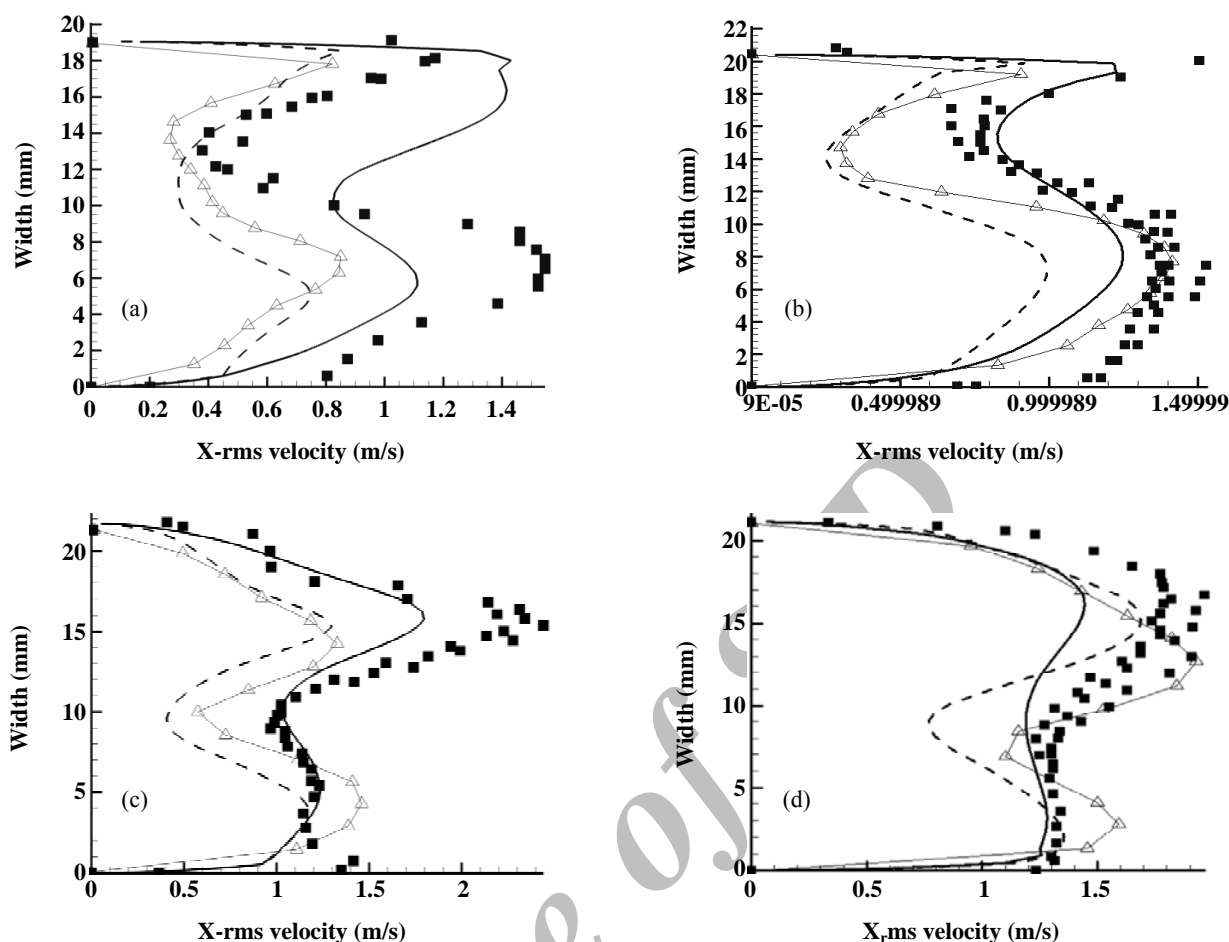
103

Fig. 8: X-rms velocity profile of the air flow inside the separator at the bulk air velocity of 3.54 m/s:
a) at x=87.5 mm   ,   b) at x= 112.5 mm   ,   c) at x=137.5 mm   ,   d) at x=165 mm.

the droplets can move through a straight line inside the separator and can escape from the separator.

Droplet Tracking Results

For each droplet size in the interested range, number of injected droplets was selected in the manner that the ratio of the droplets flow rate to the air flow rate was less than 10 percent. Velocity of the droplets is set to be equal with the mean velocity of the air field at their injection point. It is assumed that once a droplet collides with the wall, it is removed from the air flow and no rebound occurs. The Rosin-Rammler distribution was used for the droplet size at the inlet (see, for example *James et al.* [10]). The number probability density function is

$$P_n(d) = \frac{Cd^{C-4}}{\bar{d}^{C-3}\Gamma(1-\frac{3}{C})}\exp\left\{-\left(\frac{d}{\bar{d}}\right)^C\right\} \tag{48}$$

where $\bar{d}$ is the mean diameter, C is a distribution parameter and Γ denotes the gamma function. The value of C was selected so that all of the droplets have the diameter in the range of $\bar{d}-2\,\mu m < d < \bar{d}+1\,\mu m$

If droplets are divided to M size group at the separator inlet and the diameter of the droplets in the i'th size group are in the range $[d_i^s, d_i^L]$, the ratio of the number of droplets in the i'th size group to the total number of droplets at inlet is defined by

$$f_{i,0} = \int_{d_i^S}^{d_i^L} P_n(x)dx \tag{49}$$

Diameter step size of 0.05 micron has been chosen in this study ($d_i^L - d_i^S = 0.05\,\mu m$). The calculated droplet removal efficiency has been depicted in Fig. 11 for three different plate spacings at the bulk air velocity of 3.54 m/s. From this figure it can be concluded that, the separator

104

Table 4: Comparison of the calculated pressure loss with experimental data.

Case	DP [Pa]
Experimental	40.0
Un-structured quadrilateral mesh, Enhanced RSTM (Present Work)	40.09
Un-structured quadrilateral mesh, Standard RSTM (Present Work)	39.1
Structured mesh, RSTM, Law-of-the-wall (Jøsang and Melaaen (2001))	48.7
structured mesh, k-ε, Law-of-the-wall (Jøsang and Melaaen (2001))	43.1
structured mesh, k-ε, Two-layer zonal model (Jøsang and Melaaen (2001))	38.0
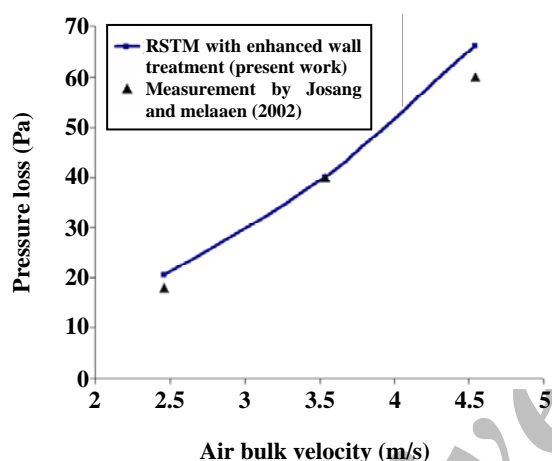
Fig. 9: The calculated pressure loss versus the air bulk velocity for 25mm plate spacing.
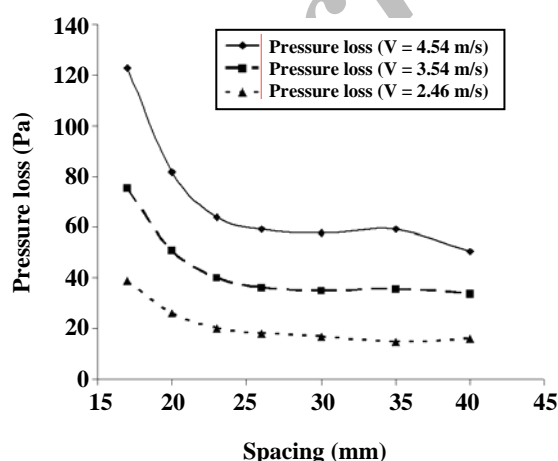
Fig. 10: The calculated Pressure loss versus plate spacing for three different air bulk velocities.

with 25 mm plate spacing has higher removal efficiency than two other separator.

By increasing the plate spacing from 25 mm to 30 mm the mean droplet size at which the removal efficiency is 95% will increase from 16 micron to 23 micron. Further increase in plate spacing from 30mm to 35mm will increase it from 23 micron to 27 micron.

By decreasing the spacing from 35 mm to 25 mm, the removal efficiency for the separator will increase but the pressure loss will remain constant. It means that for the range of the 25mm<S<35mm the spacing of the 25mm gives the best performance for the separator.

Fig. 12 shows the calculated trajectories for the droplets with the size of 4, 8, 12 and 16 micron at 25mm plate spacing for the air bulk velocity of 3.54 m/s.

This figure shows the importance of the eddy interaction model in droplet trajectory calculation. As can be seen the 8 micron droplet can escape from the separator but 4micron droplet strikes the wall. Also, the 12 micron droplet strikes the wall sooner than 16 micron droplet. This is due to the effects of velocity fluctuation in air flow which can affect the path line of the small droplets. However the probability of the collision between larger droplets and walls are more than smaller ones (See Fig. 11).

CONCLUSIONS

Air droplet flow has been numerically studied in a vane separator. First, for the examination of the developed code for gas flow simulation, its results were presented for a two-dimensional air flow inside a vane separator and compared with the experimental and numerical data from the study done by *Jøsang & Melaaen* [5-13] and *Jøsang* [23]. Then, the pressure loss and removal efficiency has been calculated and compared for different spacings between the plates of the vane separator.

Some important results from the air flow simulations and the droplet trajectory calculations are:

• By considering the wall reflection effects, RSTM can predicts the pressure loss and mean velocity profiles better than the RSTM without wall reflection effects.

• Standard RSTM predicts larger dead zone (recirculation flow region) after each the drainage channels.

• The predictions of the Enhanced RSTM for rms velocities are in better agreement with the experiments than the other versions of RSTM.
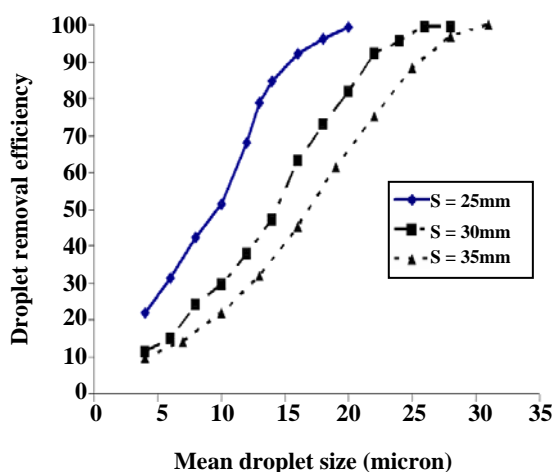
Fig. 11: The calculated droplet removal efficiency for three different plate spacings at the bulk air velocity of 3.54 m/s.
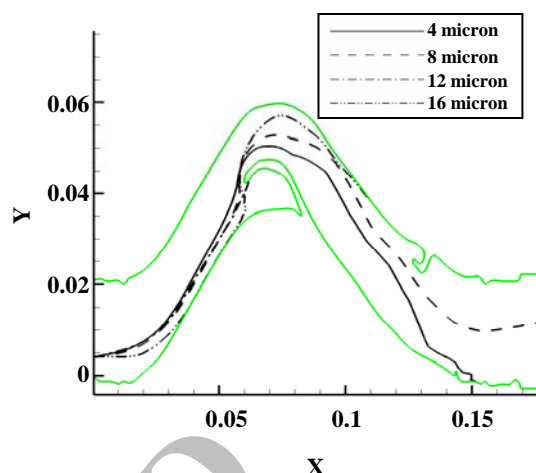

Fig. 12: The calculated trajectories for the droplets with the size of 4 micron, 8 micron, 12 micron and 16 micron at 25mm plate spacing and air bulk velocity of 3.54 m/s.

• For the plate spacings in the range of 25 mm to 35 mm, the pressure loss is approximately constant. On the other hand, the increment in plate spacing will decrease the droplet removal efficiency.

• The velocity fluctuation in air flow can affect the path line of the small droplets and change their path in the manner that they collide with the wall sooner than the heavier droplets. However, the probability of the collision between larger droplets and walls are more than smaller ones.

Nomenclature

A	Parameter for enhanced wall treatment in pressure strain term, dimensionless
A_b, A_μ	Two-layer model constants, Dimensionless
A_1, A_2, A_3	Tensor invariants, dimensionless
a_{ij}	Reynolds Stress Anisotropy Tensor, dimensionless
C_1, C_2, C'_1, C'_2, $C_{1\varepsilon}$, $C_{2\varepsilon}$, C_μ, C_L	Reynolds stress transport model constants for pressure strain term, dimensionless
C_b, C_F, C_k	Model constants for droplet distortion calculation, dimensionless
C_C	Stokes Cunningham slip correction, dimensionless
C_D	Droplet drag coefficient, dimensionless
$C_{Dsphere}$	Sphere drag coefficient, dimensionless
C^*_L	Two-layer model constant, dimensionless
C^*_{si}	Mass flux over i'th surface of the cell, kg/m^{2}s
d	Droplet diameter, μm
dij	Deformation rate tensor, L/s
E	Empirical constant for logarithmic law (9.793), dimensionless
$\vec{F}_L$	Saffman lift force vector per unit mass, m/s^2
$\vec{g}$	Gravity acceleration vector, m/s^2
G_i	Zero mean unit variance Gaussian random number, dimensionless
k	Turbulent kinetic energy, m^2/s^2
L_μ, L_ε	Length scales used in two-later model, m
L_e	Eddy length scales, m
n_k	The x_k component of the unit normal vector to the wall, dimensionless
$\vec{n}(t)$	Brownian force per unit mass, m/s^2
p	Static pressure, Pa
p'	Pressure correction, Pa
G_k	Turbulent kinetic energy production, kg/ms^2
Re	Gas flow Reynolds number, dimensionless
Re_d	Droplet Reynolds number, dimensionless
R_{et}	Turbulent Reynolds number, dimensionless
R_{ey}	Turbulent Reynolds number for two-layer, dimensionless
R_{ij}	Reynolds stress tensor, m^2/s^2
S	Plate spacing, m

106

$\vec{S}$	Surface vector, m^2
S_φ	Source term in transport equation
S_x, S_y	Surface vector components, m^2
t	Time, s
T_e	Eddy time scale, s
T_i	Interaction time, s
U_k	Air flow mean velocity components, m/s
u'	Air flow fluctuating velocity components, m/s
$\vec{u}_g$	Air flow velocity vector, m/s
$\vec{v}_d$	Droplet velocity vector, m/s
u^*	Dimensionless velocity profile
$u^*_{laminar}$	Dimensionless velocity profile in laminar sub-layer
$u^*_{trrbulent}$	Dimensionless velocity profile in logarithmic sub-layer
$\vec{x}_d$	Droplet position vector, m
y^*	Wall unit, dimensionless
y_{CD}	Droplet distortion, dimensionless

Greek

Ω_0, Ω_i	Area of the computational cell, m^2
δ_{ij}	Kronecker delta, dimensionless
Δt	Time step, s
ε	Dissipation rate, m^2/s^3
η	Droplet removal efficiency, dimensionless
κ	von Kármán constant, (0.4187), dimensionless
λ	Molecular mean free path, m
λ_ε	Blending function in two-layer model, dimensionless
μ	Molecular dynamic viscosity, kg/ms
μ_t	Turbulent dynamic viscosity, kg/ms
$\mu_{t,2layer}$	Turbulent dynamic viscosity for two-layer model, kg/ms
ρ, ρ_g	Air density, kg/m^3
ρ_d	Droplet density, kg/m^3
σ_k	Prandtl number of turbulent kinetic energy, dimensionless
σ_ε	Prandtl number of dissipation rate, dimensionless
τ_d	Droplet relaxation time, s
Γ_φ	Diffusion coefficient in transport equation
Γ	Blending function for enhanced wall treatment, dimensionless
φ	General variable in transport equation
φ_{ij}	Pressure strain term, kg/ms^2
φ_{ij1}	Slow pressure strain term, kg/ms^2
φ_{ij2}	Rapid pressure strain term, kg/ms^2
φ_{ijw}	Wall reflection pressure strain term, kg/ms^2

REFRENCES

[1] Verlaan C.C.J., Performance of Nvel Mst Eiminators, Ph.D. Tesis, Delft Univ. of Technol., Faculty of Mech. Eng. and Mar. technol, ISBN 90-370-0054-1 (1991).

[2] Wang W., Davies G.A., CFD Studies of Separation of Mists From Particles Using Vane Type Separators, *Trans. IChemE, Part A, Chem. Eng. Res. Des.*, **76**, 980 (1996).

[3] Galletti Ch., Brunazzi E., Tognotti, L., A Numerical Model for Gas Flow and Droplet Motion in Wave-Plate Mist Eliminators with Drainage Channels, *Chem. Eng. Sci.*, **63**, 5639 (2008).

[4] Ghetti S., Investigation of Entrainment Phenomena in Inertial Separators. MS Thesis, Univ. of Pisa, Pisa, Italy (2003).

[5] Jøsang A.I., Melaaen M.C., "Detailed Measurements and Simulations of a Vane Separator", Int. Conf. on Appl. Computational Fluid Dynamics, October 17-20, Beijing, China (2000).

[6] Kallio G.A., Reeks M.W., A Numerical Simulation of Particle Deposition in Turbulent Boundary layers, *Int. J. Multiphase Flow*, **15(3)**, 433, (1989).

[7] Sommerfeld M., Kohnen G., Ruger M., Some Open Questions and Inconsistencies of Lagrangian Particle Dispersion Models, Ninth Symp. Turbulent Shear Flows, Kyoto, Japan, 16-18 August (1993).

[8] Wang Y., James P.W., Assessment of an Eddy Interaction Model and its Refinements Using Predictions of Droplet Deposition in a Wave Plate Vane separator, *Trans. IChem E, Part A, Chem. Eng. Res. Des.*, **77**, 692, (1999).

[9] James P.W., B.J. Azzopardi, Y. Wang, J.P. Hughes, The Role of Drainage Channels in the performance of Wave Plate Mist Eliminators, *Trans. IChem E., Part A, Chem. Eng. Res. Des.*, **81**, 639, (2003).

[10] James P.W., Azzopardi B.J., Wang Y., Hughes J. P., A Model for Liquid Film Flow and Separation in a Wave Plate Mist eliminator, *Trans. IChem E., Part A, Chem. Eng. Res. Des.*, **83(A5)**, 469, (2005).

[11] Launder B.E., Spalding D.B., the Numerical Computation of Turbulent Flows, *Comp. Meth. Appl. Mech. Eng.*, **3**, 269, (1974).

107

[12] Rafee R., Rahimzadeh H., Ahmadi G., Numerical Simulations of Airflow and Droplet Transport in a Wave-Plate Mist Eliminator, *Chem. Eng. Res. Des.*, **88**, p. 1393 (2010).

[13] Jøsang A.I., Melaaen M.C., "Fluid Flow Simulation of Vane Separator", 42nd Scandinavian Conf. on Simulation and Modeling, Porsgrunn, Norway, October 8-9, (2001).

[14] Launder, B.E., Shima N., Second-Moment Closure for the Near-Wall Sublayer: Development and Application, *AIAA J.*, **27(10)**, 1319, (1989).

[15] Launder B.E., Second-Moment Closure: Present … and Future? *Int. J. Heat Fluid Flow*, **10(4)**: 282-300, (1989).

[16] Lien F.S., Leschziner M.A., Assessment of Turbulence-Transport Models Including Non-Linear RNG Eddy-Viscosity Formulation and Second-Moment Closure for Flow over a Backward-Facing Step, *Computers Fluids*, **23(8)**: 983-1004, (1994)

[17] Lien F.S., A Pressure Based Unstructured Grid Method for All Speed Flows, *Int. J. Numerical Methods Fluids*, **33**, 355, (2000).

[18] Rafee R., Rahimzadeh H., A New Method for Constructing the Coefficients of Pressure Correction Equation for Collocated Unstructured Grids, *Am. J. Appl. Sci.* **6(1)**, 93, (2009).

[19] Patankar S.V., "Numerical Heat Transfer and Fluid Flow", McGraw-Hill, New York, pp: 126-131, (1980).

[20] Jongen T., Simulation and Modeling of Turbulent Incompressible Flows, Ph.D. thesis, EPF Lausanne, Lausanne, Switzerland, (1992).

[21] Wolfstein M., The Velocity and Temperature Distribution of One-Dimensional Flow with Turbulence Augmentation and Pressure Gradient, *Int. J. Heat Mass Transfer*, **12**, 301, (1969).

[22] Kader B., Temperature and Concentration Profiles in Fully Turbulent Boundary Layers, *Int. J. Heat Mass Transfer*, **24(9),** 1541, (1981).

[23] Jøsang A.I., Numerical and Experimental Studies of Droplet-Gas Flow, Ph.D. Thesis, Dep. of Technol. (HiT-TF), Telemark Univ. Coll. , Norway, (2002).

[24] Chan J.K., Golay M.W., "Comparative Evaluation of Cooling Tower Drift Eliminator Performance", Dep. of Nuclear Eng. of Massachusetts Inst. of Technol. Cambridge, Massachusetts, (1977).

[25] Zhao J., Jin, B., Zhong Z., Study of the Separation Efficiency of a Vane Separator Vane with Response Surface Methodology, *J. Hazard. Mater.* ,**147**, 363, (2007).

[26] He Ch., Ahmadi G., Particle Deposition in a Nearly Developed Turbulent Duct Flow with Electrophoresis, *J. Aerosol Sci.* **30(6)**, 739, (1999).

[27] Liu A.B., Mather D., and Reitz R.D., Modeling the Effects of Drop Drag and Breakup on Fuel Sprays, *SAE Technical Paper 930072, SAE*, (1993).

[28] Hinds W.C., "Aerosol Technology: Properties, Behavior, and Measurement of Airborne Particles", Wiley, NewYork, (1982).

[29] Lamb H., "Hydrodynamics", Sixth Edition, Dover Publications, New York, (1945).

[30] Saffman P.G., The Lift on a Small Sphere in a Slow Shear Flow, *J. Fluid Mech.* **22**, 385, (1965).